Proc. Natl. Acad. Sci. USA
Vol. 91, pp. 4604–4608, May 1994
Neurobiology

Cable properties of a straight neurite of a leech neuron probed by a voltage-sensitive dye

(dendrite/membrane potential/fluorescence)

PETER FROMHERZ AND CARSTEN O. MÜLLER

Abteilung Biophysik der Universität Ulm, D-89069 Ulm, Germany

Communicated by B. Sakmann, January 31, 1994 (received for review September 13, 1993)

ABSTRACT **We measured a time-resolved map of electrical activity in a thin straight neurite (1.5 μm thick, 500 μm long) at a resolution of 8 μm and 0.4 ms. The neurite was obtained by guided outgrowth of an identified neuron of the leech on lanes of extracellular matrix protein. The electrical signals were detected by a fluorescent voltage-sensitive dye. We observed the voltage that was caused by an action potential elicited at the soma and by a Gaussian hyperpolarization induced at the soma, respectively. We compared the data with numerical solutions of the cable equation using the Hodgkin–Huxley parametrization. We could attribute the experimental results of depolarization and of hyperpolarization to the propagation of an action potential along an "active" cable and to the spread along a "passive" cable, respectively, if we assigned rather high specific resistances to the cytoplasm (R_I = 250 Ω·cm) and to the membrane (R_M = 22 kΩ·cm²). This assignment explained the slow velocity of 150 μm/ms of a pulse by active propagation and the limited range of 200 μm of a pulse by passive spread.**

It is an open question whether neural dendrites are linear electrical elements obeying the "passive" cable equation (1, 2) or whether they perform computations with "active" voltage-gated conductances (3–5). The nature of signal processing can be elucidated only by direct mapping of the membrane voltage at a resolution of ≈1 μm and 0.5 ms—the size of synapses and the rise-time of action potentials. The method of choice seems to be optical recording with voltage-sensitive dyes (6–9). Transient electrical activity—with a time constant of ≈0.5 ms—was observed at spatial resolutions of 40 μm (10–14), of 15 μm (15), and of 8 μm (16, 17). Images at a resolution of 1 μm were measured only at a time scale of ≈1 s (18).

A straight unbranched neurite is the simplest system in which to investigate transient patterns of voltage. We report here a complete voltage map of a straight 500-μm-long and 1.5-μm-thick neurite at a resolution of 8 μm and 0.4 ms. We extended a set-up for local optical recording (16) to be applied to a linear neurite obtained by guided outgrowth (19). We compared the results with numerical solutions of the cable equation and obtained the pertinent electrical parameters of the neurite.

MATERIALS AND METHODS

Neurons. We prepared an aqueous protein extract of the extracellular matrix of *Hirudo medicinalis* (20) and spread it on a coverslip. The dry protein was illuminated by a mercury high-pressure lamp through a mask of aluminum stripes (width 10 μm) on silica (P.F. and H. Schaden, unpublished work). A flexiperm chamber (Heraeus, Hanau, F.R.G.) was attached and filled with L-15 medium/glucose/fetal calf serum/gentamycin (16, 20). Identified neurons were isolated from the leech (21) and distributed in the chamber. Straight neurites grew along the lanes of active extracellular-matrix protein. We stained the neurons with the styryl-dye RH421 (22) using stained lipid vesicles (16, 23). The soma was impaled by a microelectrode (resistance 10 MΩ) and kept at a voltage of about −60 mV.

Optical Recording. The chamber was placed onto the stage of an inverted microscope (Axiomat; Zeiss). The neuron was illuminated by a mercury lamp (HBO 100 W/2; Osram, Berlin) through an interference filter (541 nm; Schott Mainz, F.R.G.) and a dichroic beam splitter (FT 580 nm; Zeiss) using an adapted Neofluar 100×/1.3 Oel (total magnification ×175) (16). The neuron was projected onto a 10 × 10 photodiode array (MD 100-2; Centronic, Croydon, U.K.) through a long-pass filter (RG 590; Schott). It was adjusted by superposition of a video picture and a calibrated drawing of the diodes (visual field of a diode 8 μm × 8 μm). Beam splitter and filters were selected to match the spectral sensitivity of RH421 (24). The 100 outputs were fed into current–voltage converters (OPA 121; Burr-Brown, Filderstadt, F.R.G., with 100-MΩ feedback resistors, time constant 0.4 ms) and eventually into differential sample-and-hold amplifiers. Ten diodes were selected, and their signals were stored on a tape recorder (Racal, Bergisch Gladbach, F.R.G.).

The protocol of a measurement was as follows: (*i*) Adjustment of a segment of the neurite along a row of 10 diodes, (*ii*) record baselines in the dark, (*iii*) record fluorescence with open shutter (after a 5-ms interval) and then switch to the sample-and-hold mode with the total fluorescence as a reference. (*iv*) Record and store fluorescence with electrical stimulation for 70 ms: A positive current (2–4 nA) was injected for 25 ms to elicit an action potential (amplitude 60–75 mV). After an interval of 10 ms, a negative Gaussian voltage (amplitude around −100 to −160 mV) was induced by a negative and positive current pulse. (*v*) After an interval of 5 s the fluorescence without stimulation was recorded for 70 ms and stored (baseline of bleaching). To overcome the limited range of the diode array (≈85 μm) we displaced the neuron along a row of diodes several times—starting with the terminal segment—and repeated cycles (*i–v*). A complete set of data was sampled from the tape at an interval of 0.1 ms and a resolution of 12 bit and read into a microcomputer. The fluorescence changes without stimulation were fitted by an exponential function and subtracted from the changes with stimulation; the results were divided by the total fluorescences. The transients of depolarization were corrected for the decreased amplitude of the action potential (from 75 to 60 mV) during a set of measurements with displaced neurites. Then all transients of depolarization were normalized to constant amplitude. The transients of hyperpolarization were scaled by the same factors. Finally the signals were smoothed

The publication costs of this article were defrayed in part by page charge payment. This article must therefore be hereby marked "*advertisement*" in accordance with 18 U.S.C. §1734 solely to indicate this fact.

Abbreviation: N cell, nociceptive neuron.

by averaging over five adjacent data points in time and by a weighted average (1:2:1) of three adjacent diodes. The array of data points at a spacing of 8 μm and 0.1 ms was used as a basis to draw contour plots of the space–time pattern of fluorescence change.

Scaling. Fluorescent voltage-sensitive dyes are linear molecular voltmeters without scale. The observed relative change of fluorescence $\Delta F(x)/F(x)$ at a position x of the neurite depends on the local change $\Delta V(x)$ of voltage, on the local sensitivity $S(x)$ of the dye and on the fraction $a_S(x)$ of fluorescing molecules that are sensitive with $\Delta F(x)/F(x) = a_S(x)\ S(x)\ \Delta V(x)$. Because $S(x)$ and $a_S(x)$ are unknown, we cannot measure the voltage profile $\Delta V(x)$. A relative voltage profile could be determined if $a_S(x)$ and $S(x)$ were constant along a neurite. However, the sensitivity $S(x)$ may vary due to a changing environment, and the fraction of sensitive dye $a_S(x)$ may vary due to a changing background fluorescence.

To overcome these problems we used two approaches: (*i*) We considered only the shape of the local transients disregarding the local scaling factors $a_S(x)\ S(x)$—i.e., we normalized all local transients with respect to their maximum. The normalized fluorescence reflects the shape of the voltage transient as $\Delta F(x)/\Delta F(x)_{max} = \Delta V(x)/\Delta V(x)_{max}$. We used this approach to evaluate the transients of depolarization. (*ii*) We considered the ratio of two different signals at the same site. The ratio of fluorescence change at each site reflects the ratio of voltages $\Delta F_2/\Delta F_1 = \Delta V_2/\Delta V_1$ independent of the local scaling factor. We used this procedure to evaluate the transients of hyperpolarization: We divided the signals of hyperpolarization by those of depolarization (25). In other words, we scaled them by the same factors used to normalize the signals of depolarization.

Phototoxicity. The amplitude of the action potential in the soma—measured by the microelectrode—dropped during the measurements by ≈20%, and the width of the pulse was slightly broadened due to a phototoxic effect of the dye. As we displaced the row of diodes from the tip of the neurite toward the soma, we obtained optical records of the action potential that were slightly narrower near the tip. We found the phototoxic effect damaged also parts of the neuron that were not illuminated.

RESULTS

We studied fluorescence transients in several sensory neurons of the leech and in Retzius cells. We present one representative set of data for a nociceptive neuron (N cell).

Straight Neurite. A microphotograph of a cultivated N cell is shown in Fig. 1. Several neurites are grown along parallel lanes of active extracellular-matrix protein. One of them was adjusted to pass the areas of detection of a row of photodiodes (8 μm × 8 μm), as marked in Fig. 1. Its length is ≈520 μm, and its diameter is ≈1.5 μm with some extended varicosities. We attained complete probing of the neurite with 63 diodes by eight overlapping displacements with respect to a row of 10 diodes. Two additional diodes probed the axon stump and the soma.

Action Potential. An action potential was elicited in the soma by a depolarizing current injection. This voltage transient induced a fluorescent transient in the soma, in the axon stump, and all along the neurite. The normalized change of fluorescence recorded by the 65 diodes is shown as a space–time map in Fig. 2*a*. Three selected traces are plotted in Fig. 2*b*. The subthreshold component of the stimulus at the soma (upper trace in Fig. 2*b*) is damped in distal parts of the neurite (lower traces in Fig. 2*b*). The action potential propagates all along the neurite. The increase and the decrease of the local depolarization are delayed in the periphery by ≈3 ms—i.e., at any given time the neurite is not isopotential. The space–time path of the peak has a peculiar sigmoid shape as seen in Fig. 2*a*: The peak has a velocity of ≈150 μm/ms in the central part of the neurite. The velocity is greater at both ends.

Hyperpolarization. The gating of the sodium conductance of leech neurons cannot be inactivated completely by tetrodotoxin (26, 27). Thus, we were not able to check directly whether the action potential pervades the neurite by active propagation or by passive spread. As a substitute, we probed the passive properties of the neurite by applying a hyperpolarizing voltage transient to the soma with a similar shape as an action potential. We chose an amplitude of about −160 mV to obtain a sufficiently strong signal in the distal parts of the neurite. The fluorescence signals were scaled at each site with respect to depolarization. They are shown as a space–time map in Fig. 2*a*. Three selected traces are plotted in Fig. 2*b*. The negative transient is damped efficiently along the neurite. It pervades the neurite only up to ≈200 μm. The width of the transient is enhanced significantly in distal parts of the neurite. Closer inspection shows that damping is not smooth—i.e., the neurite is inhomogeneous with respect to its electrical properties. A correlation of the electrical inhomogeneity and of the structural inhomogeneity seen in Fig. 1 is not found.

All observations in neurites of different N cells as well as in neurites of other sensory neurons and of Retzius cells were

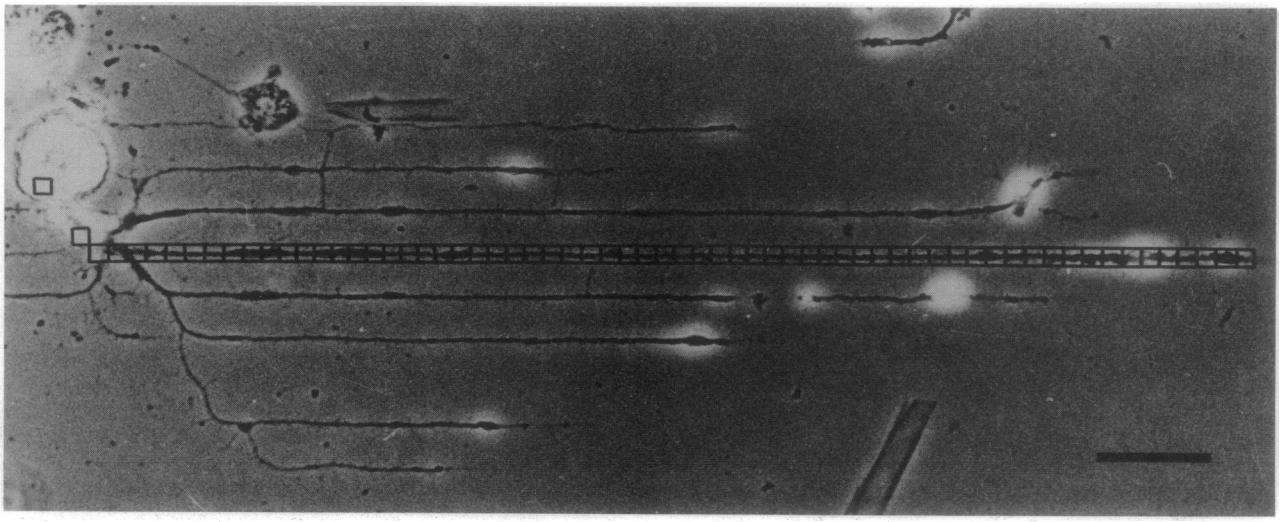

FIG. 1. Phase-contrast microphotograph of an N cell of *H. medicinalis* grown in culture on linear lanes of extracellular-matrix protein. Squares mark the position of the 65 recording diodes. (Bar = 50 μm.)

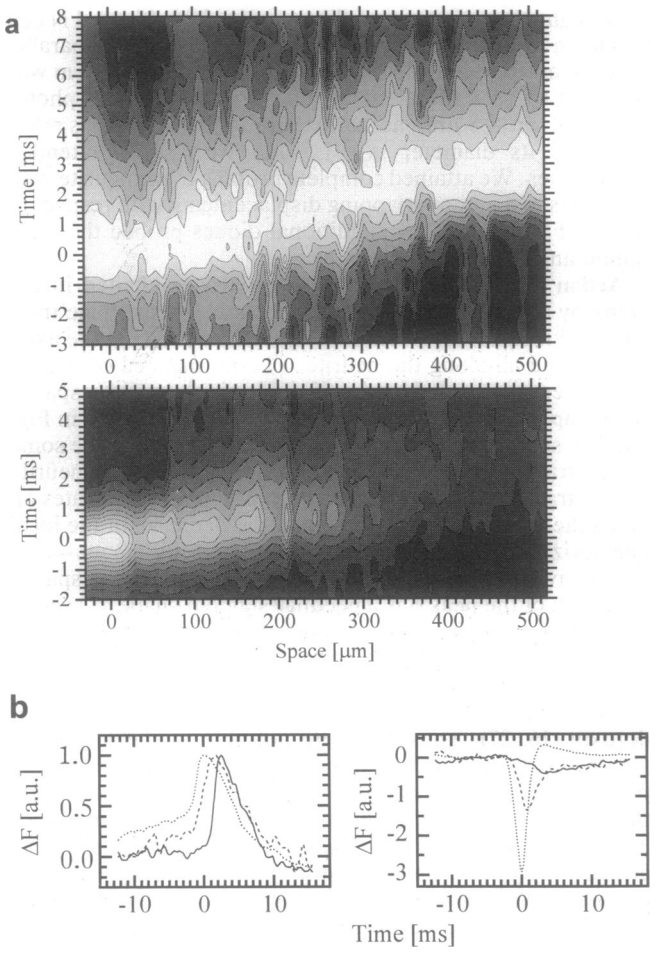

FIG. 2. Space–time patterns of fluorescence change in the neurite of an N cell. (*a*) Equidistant contour plots. The origin of space corresponds to the third diode from the left in Fig. 1. The origin in time corresponds to the maximum of the transient at the origin of space. (*Upper*) Negative fluorescence change (nine levels) induced by depolarizing current injection into the soma. The amplitudes are normalized. (*Lower*) Fluorescence change (12 levels) induced by a hyperpolarizing voltage transient in the soma. The changes are scaled by the same factors used to normalize the signals of depolarization. (*b*) Selected traces of fluorescence change (ΔF in arbitrary units) versus time in the soma (· · ·), 234 μm from the soma (- - -), and 509 μm from the soma (——). (*Left*) Depolarization. (*Right*) Hyperpolarization.

qualitatively similar to those shown in Fig. 2 with respect to shape, velocity, and damping of depolarizing and hyperpolarizing pulses.

DISCUSSION

We attempt a semiquantitative interpretation of the fluorescence experiments by comparing them with the theory of a homogeneous cable with ohmic and voltage-gated conductances (passive and active cable).

Cable Equation. The membrane voltage $V(x,t)$ as a function of space and time along a homogeneous cable is described by Eq. 1 according to a standard formulation as introduced for the giant axon of the squid (28).

$$\frac{\partial V}{\partial t} - D\frac{\partial^2 V}{\partial x^2} = -\frac{G_{Na}}{C}(V - V_{Na}) - \frac{G_K}{C}(V - V_K) - \frac{G_L}{C}(V - V_L). \quad [1]$$

The spread constant $D = d/4R_IC$ depends on the diameter d of the cable, on the specific resistance R_I of the core and on the specific capacitance C of the coat. G_{Na} and G_K are the specific conductances of the coat for sodium and potassium. G_L is the leak conductance. V_{Na}, V_K, and V_L are the reversal voltages. The sodium and potassium conductances depend on the maximal conductances G^0_{Na} and G^0_K and on the gating variables m, h, and n as $G_{Na} = G^0_{Na}\,m^3h$ and $G_K = G^0_K\,n^4$. The gating variables are governed by a voltage-dependent dynamics (28). If the dynamics of gating is suppressed with the gating variables kept at their values m_R, h_R, and n_R in the resting state, we obtain Eq. 2 for a "passive" cable with the resting voltage V_R and the time constant in the resting state $\tau = R_MC$, where $R_M = 1/(G^0_{Na}\,m^3_Rh_R + G^0_K\,n^4_R + G_L)$ is the specific membrane resistance in the resting state. Note that the electrotonic length constant in the resting state is $\lambda = \sqrt{D\tau} = \sqrt{d\,R_M/4R_I}$.

$$\frac{\partial V}{\partial t} - D\frac{\partial^2 V}{\partial x^2} = -\frac{1}{\tau}(V - V_R). \quad [2]$$

"Squid Cable." In a first approach we assign the standard electrical parameters of the squid axon (28) to a cable of diameter $d = 1.5$ μm. With the conductances $G^0_{Na} = 120$ mS/cm², $G^0_K = 36$ mS/cm², and $G_L = 0.3$ mS/cm² and the gating parameters $m_R = 0.0529$, $h_R = 0.596$, and $n_R = 0.318$ we obtain a specific membrane resistance $R_M = 1/G_M = 1.47$ kΩ·cm². The time constant is $\tau = 1.47$ ms—choosing a standard value $C = 1$ μF/cm² for the capacitance. With the core resistance $R_I = 35.4$ Ωcm we obtain a spread constant $D = d/4R_IC = 1.06$ cm²/s and an electrotonic length constant $\lambda = 395$ μm. We integrated the cable equation for a sealed 520-μm-long cable (*i*) with active gating dynamics after stimulation of an action potential in an active initial segment of 50-μm length (5), (*ii*) with active gating dynamics after imposing a hyperpolarizing Gaussian voltage in the initial segment of the cable, and (*iii*) with the gating variables kept in their resting state after stimulation of an action potential in the active initial segment. The numerical results of the first and third cases are shown in Fig. 3.

The propagation of the action potential is almost instantaneous all along the cable with a velocity > 1000 μm/ms, in

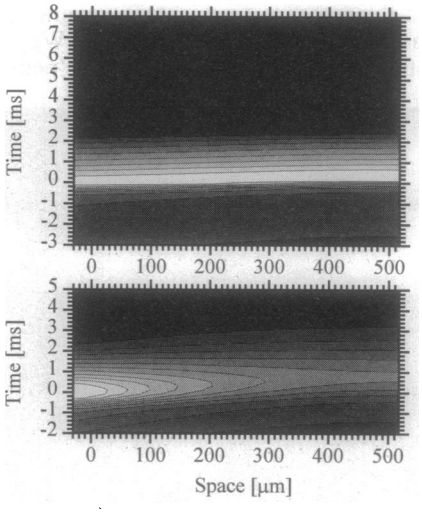

FIG. 3. Space–time pattern of voltage computed for a homogeneous cable (diameter 1.5 μm) with the electrical properties of the squid axon (specific resistances $R_I = 35.4$ Ω·cm of the core, and $R_M = 1.47$ kΩ·cm² of the membrane in the resting state; for other parameters see text). (*Upper*) Active cable with full Hodgkin–Huxley dynamics. (*Lower*) Passive cable with the sodium and potassium conductances kept in their resting state.

striking contrast to the slow propagation of the fluorescence transient of depolarization with fast phases at both ends. The range of a pulse by passive spread is similar to that of the fluorescence transient of hyperpolarization.

Matched Cable. The velocity of an action potential is controlled mainly by the spread constant D. A reduction of D, however, would reduce also the length constant $\lambda = \sqrt{D\tau}$, which restricts passive spread. To slow down the action potential and to keep the range of passive spread we have to balance a reduced spread constant $D = d/4R_IC$ by an enhanced time constant $\tau = R_MC$. We use higher values for R_I and R_M. We found an adequate similarity of theory and experiment by choosing a core resistance $R_I = 250\ \Omega$cm that is seven times higher than in the squid axon and a coat resistance $R_M = 22\ k\Omega\cdot cm^2$ that is 15 times higher than in the squid—with $G^0_{Na} = 8\ mS/cm^2$, $G^0_K = 2.4\ mS/cm^2$, and $G_L = 0.02\ mS/cm^2$. The spread constant was $D = 0.15\ cm^2/s$, the time constant was $\tau = 22$ ms, and the electrotonic length constant was $\lambda = 576\ \mu m$. The numerical results (case *i* and *iii* mentioned above) are shown in Fig. 4.

The slow velocity of the action potential now agrees well with the fluorescence transient of depolarization. Even the sigmoid shape of propagation with fast phases at both ends is reproduced. There is some enhancement of the amplitude near the cable end that cannot be seen in the normalized experimental data, of course. The range of passive spread corresponds to the range of the fluorescence transients of hyperpolarization. A similar result was found with active gating dynamics and a hyperpolarizing pulse in the initial segment (case *ii* mentioned above).

Slight variations of the parameters R_I and R_M of the homogeneous cable lead to drastic discrepancies of theory and experiment. Thus we are confident that the present approach provides a fair estimate of the average cable properties of the leech neurites—i.e., of the high specific resistance of core and membrane. Some deviations of experiment and theory remain as seen by comparison of Fig. 2 with Fig. 4. These deviations may be due to the effects of phototoxic damage during the measurement and to intrinsic electrical inhomogeneities of the neurite. A more detailed modeling of passive spread and of active propagation by the theory of an inhomogeneous cable will be meaningful only on the basis of single-shot measurements for the total neurite at an enhanced signal-to-noise ratio.

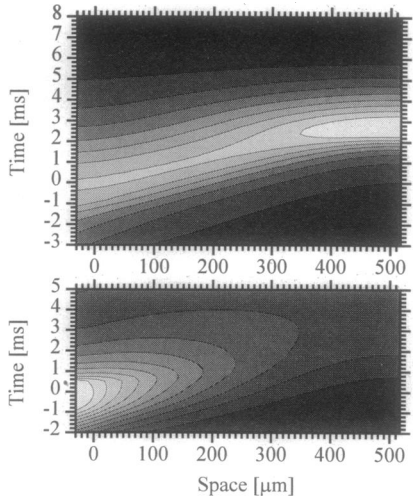

FIG. 4. Space–time pattern of voltage computed for a homogeneous cable (diameter 1.5 μm) with specific resistances $R_I = 250\ \Omega\cdot$cm of the core and $R_M = 22\ k\Omega\cdot cm^2$ of the membrane in the resting state. Best match of a homogeneous cable model to the experimental data. (*Upper*) Active cable with full Hodgkin–Huxley dynamics. (*Lower*) Passive cable with the sodium and potassium conductances kept in their resting state.

CONCLUSION

The combination of guided outgrowth and of optical recording provides a fast quasi-continuous mapping of voltage transients along a microscopic neurite. The simple geometry of the neurite allows a straightforward interpretation by the cable theory. The approach is more direct than the classical procedure to derive information about neurites from current–voltage relations measured at the soma (29–31). An application of the method to differentiated neurons of vertebrates will allow us to determine the local cable properties of dendrites.

We thank H. Schaden and T. Vetter for their help in the initial stages of this work, V. Gaede for a program to integrate the cable equation, and T. Vetter for critical reading of the manuscript. The project was supported by the Deutsche Forschungsgemeinschaft (Grant Fr 349/5).

1. Rall, W. (1977) in *Handbook of Physiology, Sect. 1: The Nervous System, Cellular Biology of Neurons* (Am. Physiol. Soc., Bethesda, MD), pp. 39–97.
2. Koch, C., Poggio, T. & Torre, V. (1982) *Philos. Trans. R. Soc. London B* **298**, 227–264.
3. Llinas, R. & Sugimori, M. (1980) *J. Physiol. (London)* **305**, 197–213.
4. Hounsgaard, J. & Midtgaard, J. (1989) *Trends Neurosci.* **12**, 313–315.
5. Fromherz, P. & Gaede, V. (1993) *Biol. Cybernet.* **69**, 337–344.
6. Salzberg, B. M., Davila, H. V. & Cohen, L. B. (1973) *Nature (London)* **246**, 508–509.
7. Cohen, L. B. & Lesher, S. (1986) *Soc. Gen. Physiol. Ser.* **40**, 71–99.
8. Grinvald, A., Frostig, R. D., Lieke, E. & Hildesheim, R. (1988) *Physiol. Rev.* **68**, 1285–1366.
9. Fromherz, P., Dambacher, K. H., Ephardt, H., Lambacher, A., Müller, C. O., Neigl, R., Schaden, H., Schenk, O. & Vetter, T. (1991) *Ber. Bunsen-Ges. Phys. Chem.* **95**, 1333–1345.
10. Grinvald, A., Ross, W. N. & Farber, I. (1981) *Proc. Natl. Acad. Sci. USA* **78**, 3245–3249.
11. Ross, W. N. & Krauthamer, V. (1983) *J. Neurosci.* **4**, 659–672.
12. Ross, W. N., Arechiga, H. & Nicholls, J. G. (1988) *J. Neurosci.* **7**, 3877–3887.
13. Parsons, T. D., Kleinfeld, D., Raccuia-Behling, F. & Salzberg, B. M. (1989) *Biophys. J.* **56**, 213–221.
14. Chien, C. B. & Pine, J. (1991) *Biophys. J.* **60**, 697–711.
15. Rohr, S. & Salzberg, B. M. (1992) *Biol. Bull.* **183**, 342–343.
16. Fromherz, P. & Vetter, T. (1991) *Z. Naturforsch. C: BioSci.* **46**, 687–696.
17. Fromherz, P. & Vetter, T. (1992) *Proc. Natl. Acad. Sci. USA* **89**, 2041–2045.
18. Gross, D., Loew, L. L. & Webb, W. W. (1986) *Biophys. J.* **50**, 339–348.
19. Fromherz, P., Schaden, H. & Vetter, T. (1991) *Neurosci. Lett.* **129**, 77–80.
20. Chiquet, M., Masuda-Nakagawa, L. & Beck, K. (1988) *J. Cell Biol.* **107**, 1189–1198.
21. Dietzel, I. D., Drapeau, P. & Nicholls, J. G. (1986) *J. Physiol. (London)* **372**, 191–205.
22. Grinvald, A., Fine, I., Farber, I. C. & Hildesheim, R. (1983) *Biophys. J.* **42**, 195–198.
23. Fromherz, P. & Röcker, C. (1994) *Ber. Bunsen-Ges. Phys. Chem.* **98**, 128–131.
24. Fromherz, P. & Müller, C. O. (1993) *Biochim. Biophys. Acta* **1150**, 111–122.
25. Sensemann, D. M., Horwitz, I. S. & Salzberg, B. M. (1987) *J. Exp. Zool.* **244**, 79–88.
26. Kleinhaus, A. L. & Prichard, J. W. (1983) *Comp. Biochem. Physiol.* **74C**, 211–218.
27. Johansen, J. & Kleinhaus, A. L. (1986) *J. Neurosci.* **6**, 3499–3504.

28. Hodgkin, A. L. & Huxley, A. F. (1952) *J. Physiol. (London)* **117**, 500–544.
29. Rall, W. (1960) *Exp. Neurol.* **2**, 503–532.
30. Nelson, P. G. & Lux, H. D. (1970) *Biophys. J.* **10**, 55–73.
31. Fleshman, J. W., Segev, I. & Burke, R. E. (1988) *J. Neurophysiol.* **60**, 60–85.